2009 IEEE International Conference on Robotics and Automation
Kobe International Conference Center
Kobe, Japan, May 12-17, 2009

Object Handling Tasks Based on Active Tactile and Slippage Sensations in a Multi-Fingered Humanoid Robot Arm

Hanafiah Yussof, *Member, IEEE*, Jiro Wada, Masahiro Ohka

***Abstract*—This paper presents a new algorithm for object handling tasks based on active tactile and slippage sensations using a humanoid robot multi-fingered arm for an object that exists at an arbitrary position. The idea is to enhance real-time object handling tasks based on tactile sensing in humanoid robotics, where grasp, move and release motions are involved. We developed a novel hemisphere-shaped optical three-axis tactile sensor to mount on fingertips of the robot arm. The tactile sensor is capable of defining normal and shearing forces simultaneously. For grasp and release motions, we designed the algorithm based on slippage direction analysis consisting of coordinate transformation of the sensing element for the arm global coordinate. The robot control system uses the analysis results to determine whether an object is in contact with the ground without needing to measure the height of the ground. The algorithm was evaluated in experiments with soft and hard objects, whereby results revealed good performance for the robot fingers in handling an object at an arbitrary position.**

I. Introduction

In real application of humanoid robots within human environments, they are required to perform certain tasks that require manipulation skills, such as finding and turning on switches, opening door knobs or locks, removing or assembling objects. Therefore, it is compulsory for humanoids to feature a dexterous object-handling ability that is based on the sense of touch or tactile sensing [1]. As demonstrated by humans, handling and manipulating objects will support humanoids in moving around safely and effectively.

Tactile sensing is defined as the process of determining physical properties and events through contact with objects in the world. As one of the five main sensing modalities in humans besides sight, sound, smell, and taste, the sense of touch will play an important role in robotic paradigms toward effective manipulation and collaboration with humans in built-for-humans environments. Nowadays, the tactile sensor is the most anticipated device for improving handling tasks because of its extreme sensitivity and capability of measuring normal and shearing forces [2~4]. In addition, material and stability recognition capabilities are advantages of a robotic arm equipped with a tactile sensor [5].

Hanafiah Yussof is with the Graduate School of Information Science, Nagoya University, Nagoya, Japan, and Universiti Teknologi MARA, Malaysia. (e-mail: hanafiah@nuem.nagoya-u.ac.jp). Jiro Wada is with the Graduate School of Engineering, Nagoya University, Nagoya, Japan (e-mail: wada@nuem.nagoya-u.ac.jp), Masahiro Ohka is with the Graduate School of Information Science, Nagoya University, Furo-cho Chikusa-ku Nagoya 464-8601 Japan (phone: +81-52-789-4251; fax: +81-52-789-4800; e-mail:: ohka@is.nagoya-u.ac.jp)

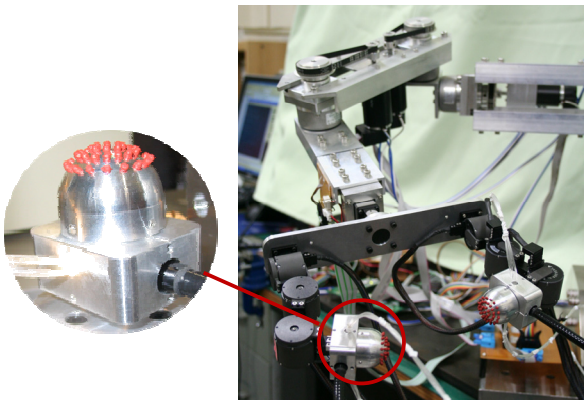

Fig.1. An 11-dofs multi-fingered humanoid arm mounted with optical three-axis tactile sensors at fingertips.

Research on tactile sensors is basically motivated by the tactile sensing system of human skin. Humans often use a combination of tactile sensation and slippage sensation to control their grasp and manipulate objects effectively. In robot handling tasks, force-gauge sensors are normally used as sensing devices in robot grippers system, especially for industrial robots. These types of sensors are mainly specialized to detect normal force. They are robust, highly sensitive with a wider range of force detection, and therefore suitable for robust handling tasks.

However, in real environments, robots are required to handle not only objects specified by humans, but also unknown objects with various stiffness and surface conditions [6]. It is very difficult for robots to control the exact grasp pressure on such objects located at an arbitrary position. Furthermore, it is too risky to perform handling tasks if the control system only relies on normal force detection. Therefore, robotic grippers require tactile sensing devices capable not only of detecting normal force, but also of measuring distribution of shearing force, so that at the same time, slippage sensation can be obtained.

In this research, to allow for better maneuvering of a humanoid robot arm toward application in a real environment, we developed a novel hemisphere-shaped optical three-axis tactile sensor. The tactile sensor is mounted on fingertips of a multi-fingered humanoid robot arm, as shown in Fig. 1. This tactile sensor uses an optical waveguide transduction method and applies image-processing techniques [7]. Such a sensing principle is expected to provide better sensing accuracy to achieve contact phenomena by acquiring the three axial directions of the forces, so that normal and shearing forces can be measured simultaneously.

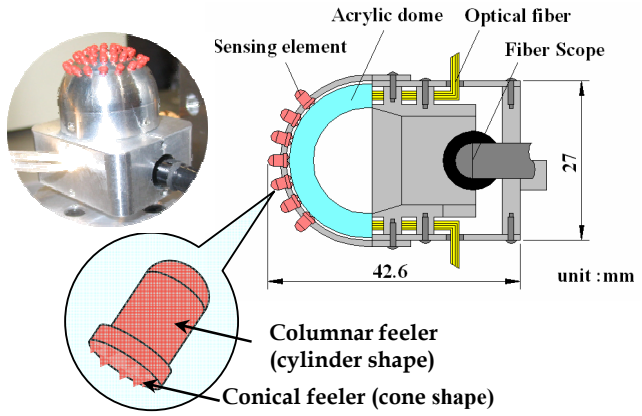

Fig. 2. Structure of optical three-axis tactile sensor and its sensing element.

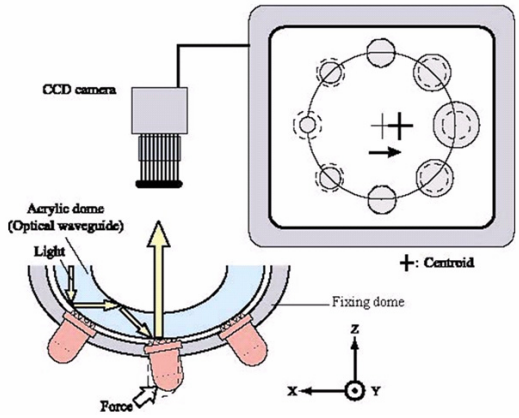

Fig. 3. Sensing principles of optical three-axis tactile sensor.

The robot arm was designed based on our humanoid robot *Bonten-Maru II* [8]. It consists of 11-dofs: 3 at the arm, 2 at wrist, and 3 at each of two fingers. In this research, we present a new control algorithm based on tactile-slippage sensation for handling an object that exists at an arbitrary position. This report is focused on the analysis of tactile-slippage sensation in the proposed algorithm in conjunction with trajectory generation of the arm. To verify the algorithm, we conduct experiments of object transferring motion using hard and soft objects with the same parameter setting, where grasp, move and release motions are involved.

II. Optical Three-Axis Tactile Sensor

The optical three-axis tactile sensor developed in this research is designed in a hemispherical dome shape that consists of an array of sensing elements. This shape mimics the structure of human fingertips for easy compliance with various shapes of objects. The hardware novelty, as shown in Fig. 2, consists of an acrylic hemispherical dome, an array of 41 pieces of sensing elements made from silicon rubber, a light source, an optical fiber-scope, and a CCD camera. The optical fiber-scope is connected to the CCD camera to acquire images of sensing elements touching the acrylic dome inside the sensor. The silicone rubber sensing element is comprised of one columnar feeler and eight conical feelers that remain in contact with the acrylic surface while the tip of the columnar feeler touches an object.

The optical three-axis tactile sensor is based on the principle of an optical waveguide-type tactile sensor. Figure 3 shows the sensing principle of the tactile sensor system. The light emitted from the light source is directed towards the edge of the hemispherical acrylic dome through optical fibers. When an object contacts the columnar feelers, resulting in contact pressure, the feelers collapse. At the points where the conical feelers collapse, light is diffusely reflected out of the reverse surface of the acrylic. Contact phenomena consisting of bright spots caused by the collapse of the feelers are observed as image data, which are retrieved by the optical fiber-scope connected to the CCD camera and transmitted to the computer.

Meanwhile, in shearing force detection, when tangential force is applied to the sensing element, the sensing element collapses according to the applied load direction. At the same time, the centroid point of the bright spot is also shifted. Therefore, the shearing force can be calculated based on horizontal displacement of this centroid point.

In the measurement process, the normal force of the F_x, F_y and F_z values are calculated using integrated gray-scale value G, while shearing force is based on horizontal center point displacement. The displacement of gray-scale distribution $\boldsymbol{u}$ is defined in (1), where $\boldsymbol{i}$ and $\boldsymbol{j}$ are the orthogonal base vectors of the x- and y-axes of a Cartesian coordinate, respectively. This equation is based on calibration experiments, and material functions are identified with piecewise approximate curves [9]. Finally, each force component is defined in (2).

$$\boldsymbol{u} = u_x\boldsymbol{i} + u_y\boldsymbol{j} \tag{1}$$

$$F_x = f(u_x),\ F_y = f(u_y),\ F_z = g(G) \tag{2}$$

III. Analysis of Tactile-Slippage Sensation

In the current study, to evaluate performance of object handling tasks using tactile sensing in a real humanoid robot system, we developed a new multi-fingered humanoid robot arm, as previously shown in Fig. 1. Distribution of the coordinate system at the robot finger and tactile sensor are shown in Fig. 4. Meanwhile, Fig. 5 shows distribution of the coordinate system at the robot arm. The global coordinate of robotic fingers (x_{FG}, y_{FG}, z_{FG}) is fixed at the centre point of the two fingers. The global coordinate for the tactile sensor (x_S, y_S, z_S) is fixed at the center of the hemispherical dome. The global coordinate for the arm (x_{AG}, y_{AG}, z_{AG}) is fixed at the intersection point of two shoulder joints.

In object transferring motion, slippage that occurred during initial grasp is the result of the object's weight resistance. It can be defined by using current object stiffness recognition in the robot control system [10]. However in release motion, slippage that occurs is the result of the object contacting with the ground surface. To avoid damaging the object or the sensing element during the release motion, the direction of slippage is measured so that the robot control system can obtain the correct timing to release the grip on the object.

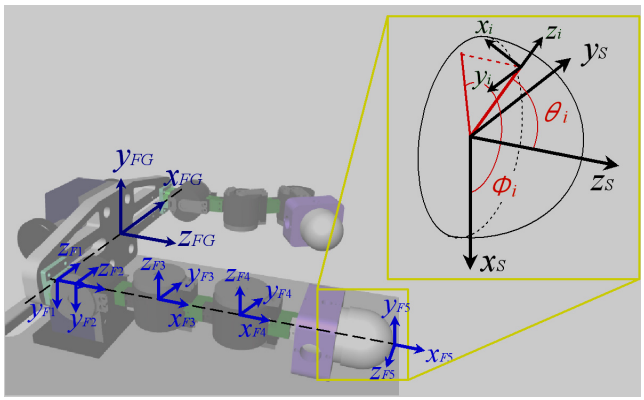

Fig. 4. Coordinate distributions at robotic finger and tactile sensor.

As previously explained, we have fixed global coordinates for the tactile sensor unit, the finger system, and the robot arm. To define slippage direction, it is necessary to perform coordinate transformation of the centroid point displacement of the integrated gray-scale value at the tactile sensor element. The coordinate transformation is calculated simultaneously from the sensor element to the sensor unit, robot fingers and finally the robot arm. In general, the direction of slippage during object lifting is to the positive side of the arm global coordinate. While the object is contacting the ground, the slippage direction is to the negative side of the arm global coordinate. Referring to Fig. 4, at first the coordinate axis of number-*i* tactile sensing element is transformed to the tactile sensor global coordinate as written in Eq. (1).

$$\begin{bmatrix} dx_S \\ dy_S \\ dz_S \end{bmatrix} = \begin{bmatrix} \cos\phi_i & -\sin\phi_i & 0 \\ \sin\phi_i & \cos\phi_i & 0 \\ 0 & 0 & 1 \end{bmatrix} \begin{bmatrix} \cos\theta_i & 0 & \sin\theta_i \\ 0 & 1 & 0 \\ -\sin\theta_i & 0 & \cos\theta_i \end{bmatrix} \begin{bmatrix} dx_i \\ dy_i \\ 0 \end{bmatrix} = \begin{bmatrix} \cos\theta_i\cos\phi_i & -\sin\phi_i & \sin\theta_i\cos\phi_i \\ \cos\theta_i\sin\phi_i & \cos\phi_i & \sin\theta_i\sin\phi_i \\ -\sin\theta_i & 0 & \cos\theta_i \end{bmatrix} \begin{bmatrix} dx_i \\ dy_i \\ 0 \end{bmatrix} \quad (3)$$

Next, the above coordinate is transformed to the finger global coordinate as follows:

$$\begin{bmatrix} dx_{FG} \\ dy_{FG} \\ dz_{FG} \end{bmatrix} = {}^{FG}_{S}\mathbf{R} \begin{bmatrix} dx_S \\ dy_S \\ dz_S \end{bmatrix} \quad (4)$$

where, ${}^{FG}_{S}\mathbf{R}$ is the rotation matrix of the tactile sensor coordinate to the robot finger coordinate. Consequently, ${}^{FG}_{S}\mathbf{R}$ is defined as following Eqs. (5) ~ (9). Here, the first frame of the finger global coordinate is rotating at θ_1 of the *y*-axis and θ_2 of the *x*-axis. Note that $c \equiv \cos$, and $s \equiv \sin$.

$${}^{FG}_{F2}\mathbf{R} = {}^{FG}_{F1}\mathbf{R}\,{}^{F1}_{F2}\mathbf{R} = \begin{bmatrix} c\phi_1 c\theta_1 + s\phi_1 s\phi_2 s\theta_1 & -c\phi_1 s\theta_1 + s\phi_1 s\phi_2 c\theta_1 & s\phi_1 c\phi_2 \\ c\phi_2 s\theta_1 & c\phi_2 c\theta_1 & -s\phi_2 \\ -s\phi_1 c\theta_1 + c\phi_1 s\phi_2 s\theta_1 & s\phi_1 s\theta_1 + c\phi_1 s\phi_2 c\theta_1 & c\phi_1 c\phi_2 \end{bmatrix} = \begin{bmatrix} a_{11} & a_{12} & a_{13} \\ a_{21} & a_{22} & a_{23} \\ a_{31} & a_{32} & a_{33} \end{bmatrix} \quad (5)$$

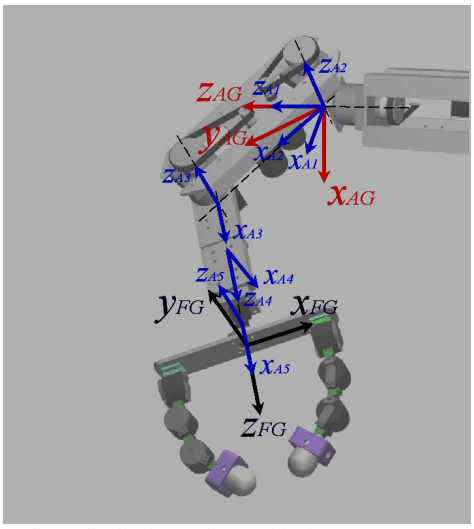

Fig. 5. Coordinate distributions at humanoid robot arm.

$${}^{FG}_{F3}\mathbf{R} = {}^{FG}_{F2}\mathbf{R}\,{}^{F2}_{F3}\mathbf{R} = \begin{bmatrix} a_{11}c\theta_2 + a_{13}s\theta_2 & -a_{11}s\theta_2 + a_{13}c\theta_2 & -a_{12} \\ a_{21}c\theta_2 + a_{23}s\theta_2 & -a_{21}s\theta_2 + a_{23}c\theta_2 & -a_{22} \\ a_{31}c\theta_2 + a_{33}s\theta_2 & -a_{31}s\theta_2 + a_{33}c\theta_2 & -a_{32} \end{bmatrix} \quad (6)$$

$${}^{FG}_{F4}\mathbf{R} = {}^{FG}_{F3}\mathbf{R}\,{}^{F3}_{F4}\mathbf{R} = \begin{bmatrix} a_{11}c(\theta_2+\theta_3) + a_{13}s(\theta_2+\theta_3) & -a_{11}s(\theta_2+\theta_3) + a_{13}c(\theta_2+\theta_3) & -a_{12} \\ a_{21}c(\theta_2+\theta_3) + a_{23}s(\theta_2+\theta_3) & -a_{21}s(\theta_2+\theta_3) + a_{23}c(\theta_2+\theta_3) & -a_{22} \\ a_{31}c(\theta_2+\theta_3) + a_{33}s(\theta_2+\theta_3) & -a_{31}s(\theta_2+\theta_3) + a_{33}c(\theta_2+\theta_3) & -a_{32} \end{bmatrix} \quad (7)$$

$${}^{FG}_{F3}5\mathbf{R} = {}^{FG}_{F3}\mathbf{R}\,{}^{F4}_{F5}\mathbf{R} = \begin{bmatrix} a_{11}c(\theta_2+\theta_3) + a_{13}s(\theta_2+\theta_3) & -a_{12} & a_{11}s(\theta_2+\theta_3) - a_{13}c(\theta_2+\theta_3) \\ a_{21}c(\theta_2+\theta_3) + a_{23}s(\theta_2+\theta_3) & -a_{22} & a_{21}s(\theta_2+\theta_3) - a_{23}c(\theta_2+\theta_3) \\ a_{31}c(\theta_2+\theta_3) + a_{33}s(\theta_2+\theta_3) & -a_{32} & a_{31}s(\theta_2+\theta_3) - a_{33}c(\theta_2+\theta_3) \end{bmatrix} \quad (8)$$

$${}^{FG}_{S}\mathbf{R} = {}^{FG}_{F5}\mathbf{R}\,{}^{F5}_{S}\mathbf{R} = \begin{bmatrix} a_{12} & -a_{11}s(\theta_2+\theta_3) + a_{13}c(\theta_2+\theta_3) & a_{11}c(\theta_2+\theta_3) + a_{13}s(\theta_2+\theta_3) \\ a_{22} & -a_{21}s(\theta_2+\theta_3) + a_{23}c(\theta_2+\theta_3) & a_{21}c(\theta_2+\theta_3) + a_{23}s(\theta_2+\theta_3) \\ a_{32} & -a_{31}s(\theta_2+\theta_3) + a_{33}c(\theta_2+\theta_3) & a_{31}c(\theta_2+\theta_3) + a_{33}s(\theta_2+\theta_3) \end{bmatrix} \quad (9)$$

Finally, the robot finger global coordinate is transformed to the robot arm global coordinate as follows:

$$\begin{bmatrix} dx_{AG} \\ dy_{AG} \\ dz_{AG} \end{bmatrix} = {}^{AG}_{FG}\mathbf{R} \begin{bmatrix} dx_{FG} \\ dy_{FG} \\ dz_{FG} \end{bmatrix}. \quad (10)$$

Here, ${}^{AG}_{FG}\mathbf{R}$ is a rotation matrix of the finger's global coordinate to the robot arm global coordinate. Eventually, the decision to loosen the grip based on the slippage direction is conducted at the robot finger controller by defining Eqs. (3) and (4). Meanwhile for Eq. (10), without kinematics information of the arm, it cannot be defined. Therefore, once the orientation of the arm is changed, the arm controller keeps sending values of ${}^{AG}_{FG}\mathbf{R}$ to the finger controller.

IV. TACTILE-SLIPPAGE BASED CONTROL ALGORITHM

In this research, we used slippage sensation obtained from shearing force distribution to control the grasp of fingers on an object located at an arbitrary position. As mentioned before, shearing force is calculated from centroid displacement of integrated-gray-scale value at the sensing elements. In this section, we present a case study of object transferring motion where grasp, move and release motions are involved. Fig. 6 shows a flowchart of communications between the arm and finger controllers in the proposed algorithm. Detailed explanations are as follows.

1. After the system begins to operate, the controller of the arm moves the arm toward the target holding position (hereafter, point A), and makes the holding orientation. The finger controller goes into a stand-by state.
2. The arm controller sends instruction to the finger controller to start the holding motion when arriving at an approximate position near the object. The finger controller begins slowly grasp the object.
3. When the fingers have defined a suitable grasp pressure on an object, the finger controller sends a 'Grasping Ended' instruction to the arm controller so that the arm can start to lift and move the object. At this moment, the finger controller switches to the 'Hold' mode. At this time, when slippage is detected caused by the movement of the arm or the object's weight, the finger controls the grip by re-pushing towards the object so that the object will not drop. Here, even if only a single value of centroid displacement exceeds the fixed threshold value, the finger controller considers that slippage has occurred. Hence the fingers refine the grip by performing a re-push motion.
4. The arm moves to the targeted position (hereafter, point B) while maintaining its orientation holding the object.
5. The arm controller sends an instruction to the finger controller to start the process of releasing the grip based on slippage information. At this time, both fingers move to the lower position (hereafter, point C) toward the ground while the arm maintains its orientation. The finger controller begins to calculate coordinate transformation while moving to point C. Finally, the object comes into contact with the ground before it reaches point C. When slippage is detected the finger will release the object.
6. When the release motion ends, the finger controller sends an instruction to the arm controller to return to point B.

During release motions, when an object touches the ground, the finger control system chooses only one sensor element that shows the maximum normal force value among sensor elements where slippage was detected. This sensor element is used as a coordinate point in coordinate transformation analysis to define the direction of slippage. The reason for this selection method is that the object seems to rotate when it comes into contact with the ground, and the sensor pin that has shown the maximum normal force value has become the center point of this rotation. Furthermore, the direction of centroid change at the sensor pins around this point of rotation may be different than the overall slippage direction of the object.

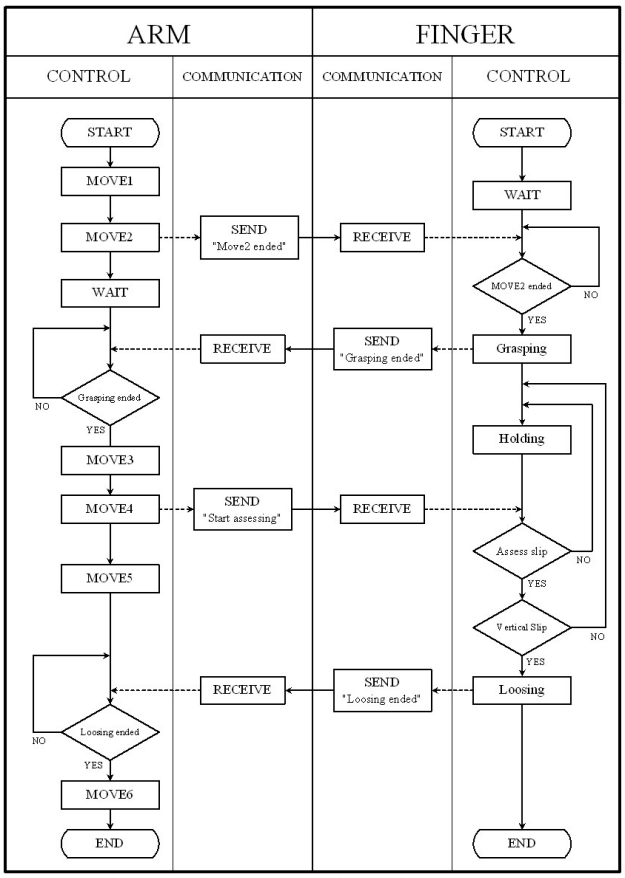

Fig. 6. Flowchart of tactile-slippage based control algorithm.

Next, when the slippage acquired from the centroid displacement value obtained from the coordinate transformation calculations exceeds the threshold value of the arm global coordinate at the x_{AG} axis element, the robot fingers start loosening their grip to release the object. At this moment, the finger controller sends a stand-by instruction to the arm controller so that the arm stops its movement toward the lower side direction. This will allow both fingers to steadily release the object onto the ground. This control algorithm allows a better maneuvering of the robot arm-finger system when handling an unknown object based on tactile sensing, particularly when handling a soft and fragile object. It also useful for handling an object located at an arbitrary position.

V. VERIFICATION EXPERIMENT AND RESULTS

We conducted a set of experiments to verify the performance of the proposed control algorithm by transferring motion of soft and hard objects located at an arbitrary position. The experiment was conducted using the multi-fingered humanoid robot arm equipped with optical three-axis tactile sensors. The objects were a cube-shaped wood block and a soft paper box. Table 1 shows the coordinate position of the fingertips at each moving point A, B and C. Table 2 shows parameters used in the robot control system for both experiments.

Table 1. Position of fingertips for each motion.

Condition of fingertip	(x_{AG}, y_{AG}, z_{AG})
Initial point	(180, 250, -100)
Point A	(185, 250, -165)
Grasping point	(220, 250, -200)
Point B	(180, 250, -100)
Contact point	(200, 250, -100)
Point C	(230, 250, -100)

Table 2 Parameter setting in object handling experiments.

Category		Parameter
Interval for Sampling	Sensing Program	100 ms
	Finger Control Program	25 ms
	Arm Control Program	25 ms
Velocity of Fingertip	MOVE1, 4	6.5 mm/s
	MOVE2, 3, 5, 6	2 mm/s
Grasping Velocity (x_{FG},y_{FG},z_{FG})	v_0 (1st finger)	(-2, 0, 0) mm/s,
	v_0 (2nd finger)	(2, 0, 0) mm/s
Re-push velocity	v_p	2 mm/s
Threshold of Centroid Displacement	dr_G (Grasping)	0.004 mm
	dr_L (Loosening)	0.004 mm
Sampling Time	t	120.0 s

About point C, actually the object will touch the ground before the fingertips reach point C. At this moment, the finger control system will perform coordinate transformation and measure slippage direction. When the detected slippage exceeds the threshold of centroid displacement, both fingers start to loosen their grip on the object and steadily release it. Figs. 7 and 8 show photographs of both experimental conditions. In both experiments, the robot arm-finger system managed to grasp, move and release the objects safely without damaging the objects or the sensor elements. Figs. 9 and 10 show the relationship between fingertip positions and slippage direction, which are calculated for the arm's global coordinate in the experiments with the paper box and wood block. In both experiments, fingers start to grasp and release the object when the slippage value exceeds the fixed threshold value. This can be observed in the graphs at the changes of fingertip movement, which correlate with the detection of slippage.

In the experiment with the paper box, as shown in Fig. 9, it was clearly demonstrated that the direction of slippage is at the positive side while grasping the object. However, during the release motion, the direction was detected toward the negative side. Both fingers started releasing their grip when the slippage exceeded the threshold value at about 70.9 second areas. In the experiment with the wood block, the directions of slippage were in both directions. This is caused by rotation of the object due to the weight to adjust its position. In this condition, the finger control system can still

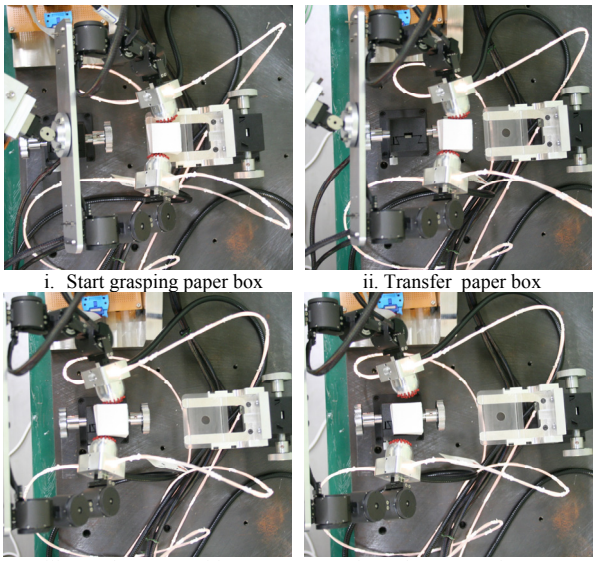

i. Start grasping paper box ii. Transfer paper box

iii. Reach target position iv. Release paper box

Fig. 7. Object handling experiment with paper box.

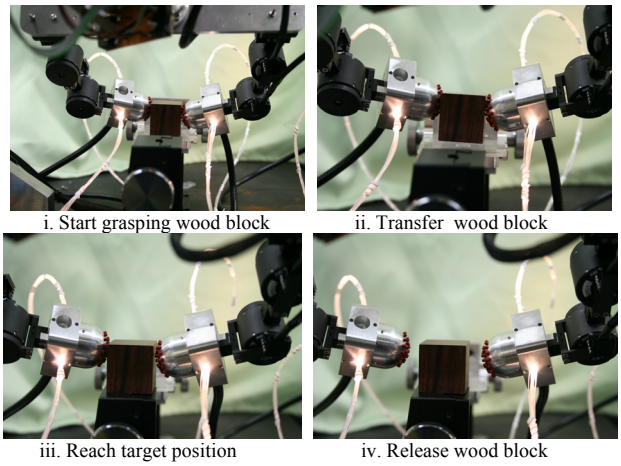

i. Start grasping wood block ii. Transfer wood block

iii. Reach target position iv. Release wood block

Fig. 8. Object handling experiment with wood block.

manage to perform grasp and release motions since the first detections of slippage are at the positive side during the grasp and at the negative side during the release motion.

This algorithm enables the robot arm-finger system to grasp and transfer an object safely without knowing the exact height of the ground to which the object is transferred. In the proposed algorithm, tactile information of both normal and shearing forces are used to control grasp pressure by adjusting the re-push velocity on the object surface based on stiffness recognition [4]. At the same time, real-time active tactile sensing information is used to generate the trajectory of the fingers. Meanwhile, the analysis results of slippage direction are used in the robot controller to measure accurately the timing of both fingers to release an object when it reaches to the targeted location. By applying this control algorithm, the robot arm-finger system is able to steadily release the object onto the ground without over pushing it, which might crush the object or damage the sensing elements. It can also automatically adapt to the stiffness of the object.

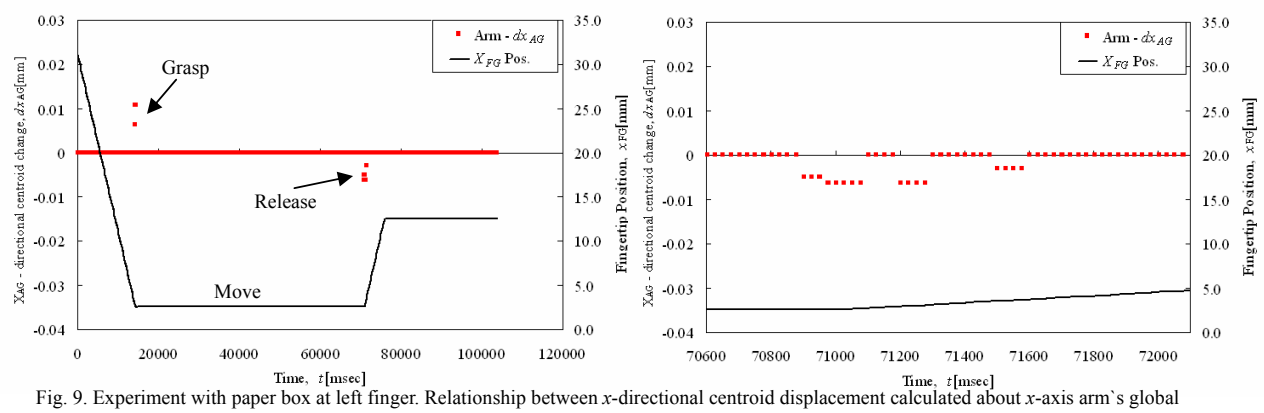

Fig. 9. Experiment with paper box at left finger. Relationship between x-directional centroid displacement calculated about x-axis arm`s global coordinate, and x-directional fingertip position. *(Left)* For all motions. *(Right)* At release motion.

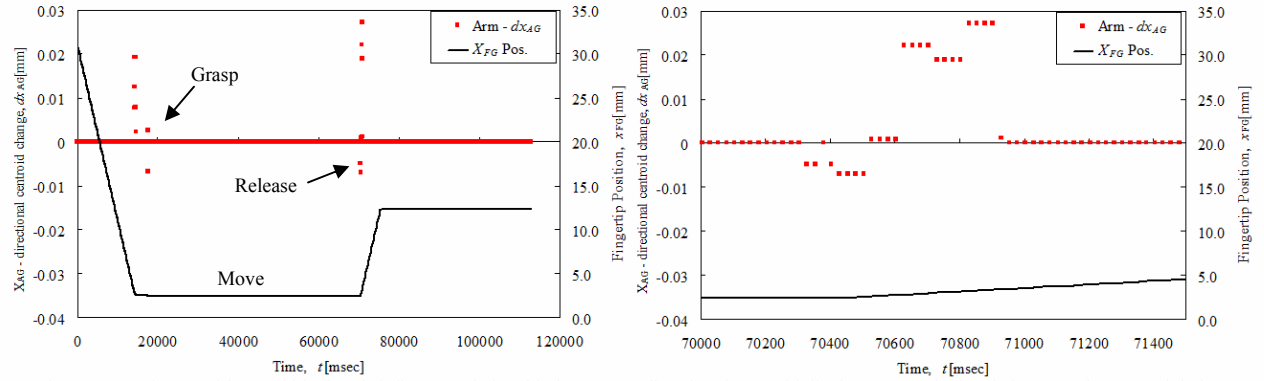

Fig. 10. Experiment with wood block at left finger. Relationship between x-directional centroid displacement calculated about x-axis arm`s global coordinate, and x-directional fingertip position. *(Left)* For all motions. *(Right)* At release motion.

VI. Conclusions

In this report, we presented a new control algorithm based on tactile-slippage sensation to define suitable grasp pressure and trajectory control during object handling tasks. We used a multi-fingered humanoid robot arm equipped with an optical three-axis tactile sensor. We presented a case study of grasp, move and release motions. To define suitable timing to lift and release an object, we conducted analysis of slippage direction based on coordinate transformation of the arm system. Finally, the performance of the proposed control algorithm was evaluated in an experiment with soft and hard objects, whereby results revealed good performance for robot fingers in defining optimum grasp pressure and in autonomously controlling the grasp and release motions of the object at an arbitrary position.

This algorithm helps the robot control system handle an object safely without needing to measure the height of the ground where an object is going to be located. It allows for better maneuvering of robotic fingers and is suitable for handling a soft and fragile object in a high risk environment, such as in nuclear plants.

Acknowledgment

A part of this study was supported by fiscal 2008-2010 Grant-in-Research by The Japan Society for the Promotion of Science (JSPS) no. P 08062.

References

[1] H. R. Nicholls and M. H. Lee, “A Survey of Robot Tactile Sensing Technology,” *Int. J. Robotics Research*, vol. 8-3, pp. 3-30, 1989.

[2] S. Omata, Y. Murayama and C.E. Constantinou, “Real time robotic tactile sensor system for determination of the physical properties of biomaterials”, *J. Sensors and Actuators A*, 112(2-3), pp 278-285, 2004.

[3] O. Kerpa, K. Weiss and H. Worn, “Development of a flexible tactile sensor system for a humanoid robot”, in *Proc. IROS2003*, vol. 1, pp. 1-6, Oct. 2003, Las Vegas, USA.

[4] M.H. Lee and H.R. Nicholls, “Tactile sensing for mechatronics: a state of the art survey”, *Journal Mechatronics*, 9(1), pp 1-31, 1999.

[5] S. Takeuchi, M. Ohka and Y. Mitsuya, “Tactile Recognition Using Fuzzy Production Rules and Fuzzy Relations for Processing Image Data from Three-dimensional Tactile Sensors Mounted on a Robot Hand,” in *Proc. of the Asian Control Conf.* , vol. 3, pp. 631-634, 1994.

[6] A. Edsinger and C. Kemp, “Manipulation in human environments”, in *Proc. Int. Conf. on Humanoid Robotics (Humanoids06)*, Italy, 2006.

[7] M. Ohka, N. Morisawa, H. Suzuki, J. Takada, H. Kobayashi and H. Yussof, “A Robotic Finger Equipped with an Optical Three-axis Tactile Sensor”, in *Proc. ICRA2008*, pp. 3425-3430, 2008.

[8] H. Yussof, M. Yamano, Y. Nasu and M. Ohka, “Performance of a Research Prototype Humanoid Robot *Bonten-Maru II* to Attain Human-Like Motion,” *WSEAS Transaction on Systems and Control*, vol. 2, Issue 9, pp. 458-467, September 2007.

[9] M. Ohka, H. Kobayashi and Y. Mitsuya, “Sensing precision of an optical three-axis tactile sensor for a robotic finger”, in *Proc. 15th IEEE International Symposium on Robot and Human Interaction Communication (RO-MAN2006)*, pp. 220-225, 2006.

[10] H. Yussof, M. Ohka, J. Takata, Y. Nasu and M. Yamano, “Low Force Control Scheme for Object Hardness Distinction in Robot Manipulation Based on Tactile Sensing,” *in Proc. ICRA2008*, pp. 3443-3448, Pasadena, CA, USA, May 19-23, 2008.